Int. J. Solids Structures Vol. 24, No. 4, pp. 351–362, 1988
Printed in Great Britain.

0020–7683/88 $3.00+.00
© 1988 Pergamon Press plc

HIGHLY NON-LINEAR DEFORMATION OF UNIFORMLY-LOADED CIRCULAR PLATES

G. WAYNE BRODLAND
Department of Civil Engineering, University of Waterloo, Waterloo, Ontario, Canada N2L 3G1

(*Received* 14 *March* 1986; *in revised form* 8 *May* 1987)

Abstract—A theory for the axisymmetric deformation of isotropic, hyperelastic circular plates which is valid for arbitrarily large strains and rotations is developed. The theory is implemented numerically and used to perform an extensive analysis of uniformly-loaded circular plates with hinged and clamped edges. Particular attention is paid to large-strain and large-rotation effects.

1. INTRODUCTION

The axisymmetric deformation of circular plates has probably been studied in more detail than any other plate problem. Even so, large-strain effects and the influence of the ratio a/h of plate radius to thickness have received little attention. Presumably, this is because most plate solutions are based on equations such as the von Karman equations, which ignore these factors. A few recent solutions such as Refs [1, 2], based on the Reissner equations[3], do, however, show the effect of a/h. In this paper, a plate theory which is valid for *arbitrarily large* strains, displacements and rotations is developed. The numerical solution of the resulting governing equations makes it possible to analyze a very wide range of deformations, including some which are well beyond the ranges for which the von Karman and Reissner equations are applicable. Large-strain effects and the importance of the ratio a/h when rotations are large are thus shown. Much of the current research on the large deflection of plates assumes elasto-plastic constitutive relations[4]. In contrast, hyperelastic behavior is assumed here.

Consider a thin circular plate of radius a and thickness h subjected to a uniform transverse load q per unit area (Fig. 1). Let the plate be made of a homogeneous, isotropic, hyperelastic material. Further assume that like most materials which can undergo large elastic strains, such as rubber, the material is incompressible. The non-linear Mooney–Rivlin model adequately describes many real materials in this class, and is assumed here. The material constants C_1, C_2 in this model can be chosen to model a wide range of linear and non-linear responses. The constants will be chosen as $C_1 = 5G/8$ and $C_2 = -G/8$, where $G = E/2(1+\nu)$, for the numerical calculations. This will allow the results to be compared with results in the literature, most of which are for linear materials. Direct comparisons can be made with those results given for incompressible materials ($\nu = 0.5$). For a review of solutions to the title problem, see Brodland[5]. The behavior of plates under clamped and hinged edge conditions will be considered in detail. The use of radially restrained edges in both cases prevents possible buckling in the hoop direction[6] due to compressive hoop stresses.

It can be shown[5] that the axisymmetric deflection of uniformly-loaded circular plates is governed by a geometric parameter, a load parameter and a material parameter. These parameters are usually defined as a/h, qa^4/Dh and ν, respectively, in terms of $D = Eh^3/12(1-\nu^2)$. Deflections w/h and membrane and bending stresses $\sigma a^2 h/D$ result. When strains are large, parameters a/h, qah^2/D and ν, which produce similar *middle surface shapes*, are more appropriate. This paper investigates the influence of the geometric and load parameters over wide ranges of their values.

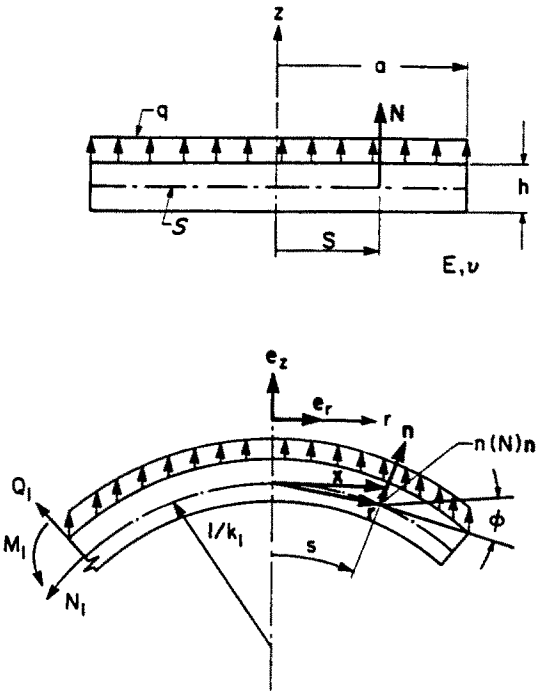

Fig. 1. Uniformly-loaded circular plate.

2. GOVERNING EQUATIONS

The non-linear deflection of plates is governed by equilibrium, strain–displacement and constitutive equations[5]. These equations are well known. Under suitable restrictions on the magnitude of strains and rotations, the above equations can be combined to yield pairs of higher-order, coupled, governing equations. See Chia[7], Donnell[8] or Reissner[3] for a discussion of particular restrictions and their resulting governing equations. The governing equations can be directly solved or they can be recast and solved using a *variational principle*. The latter approach is used here.

Consider the axisymmetric deformation of a circular plate. Assume that the deformation satisfies a relaxed Kirchhoff hypothesis; that is, particles on a normal N to the undeformed middle surface remain on their corresponding normal **n** to the deformed image of the middle surface, but their distance from the middle surface can change. This formulation allows deformations consistent with large middle surface strains, but *neglects shear strain*. Note that the deformed image of the middle surface will not, in general, correspond to the middle of the deformed plate. The deformed plate is then described by

$$\mathbf{r} = \mathrm{r}(\mathrm{s})\mathbf{e}_\mathrm{r}(\theta) + \mathrm{z}(\mathrm{s})\mathbf{e}_\mathrm{z}, \quad \mathbf{x} = \mathbf{r} + \mathrm{n}(\mathrm{N})\mathbf{n} \tag{1}$$

where **r** is the position vector to an arbitrary point on the deformed middle surface; **n** is a unit outward normal to the deformed middle surface s, given by

$$\mathbf{n} = \cos\phi\ \mathbf{e}_\mathrm{z} + \sin\phi\ \mathbf{e}_\mathrm{r} \tag{2}$$

in terms of the angle ϕ between the meridional tangent and $\mathbf{e}_\mathrm{r}$; and **x** gives the position of an arbitrary point initially at position N through the plate thickness (Fig. 1). Equations (1) and (2) are written in terms of a cylindrical coordinate system $(\mathrm{r}, \theta, \mathrm{z})$ which has associated orthonormal basis $(\mathbf{e}_\mathrm{r}, \mathbf{e}_\theta, \mathbf{e}_\mathrm{z})$. Surface coordinates (s, θ) measure arc length along a meridian and along a parallel circle, respectively, and correspond to the lines of curvature on s. The distance n to an arbitrary point at x is measured along **n** from the deformed middle surface

s. The undeformed configuration S is distinguished from the deformed configuration s by the use of upper case symbols, and is given by

$$\mathbf{R} = S\mathbf{e}_r, \quad \mathbf{X} = \mathbf{R} + N\mathbf{e}_z, \quad \Phi = 0. \tag{3}$$

The deformation is made mathematically explicit by assuming that S maps onto s and by specification of

$$s = s(S), \quad \theta = \Theta, \quad n = n(N). \tag{4}$$

We note that the principal stretches v_i are easily calculated as

$$v_1 = (1 + k_1 n)\lambda_1, \quad v_2 = (1 + k_2 n)\lambda_2, \quad v_3 = dn/dN \tag{5}$$

in terms of the principal stretches λ_α, $\alpha = 1, 2$ in the meridional and hoop directions, respectively, and curvatures k_α of the deformed middle surface s. These deformation measures are given in turn by

$$\lambda_1 = \frac{ds}{dS}, \quad \lambda_2 = r/R \tag{6}$$

and

$$k_1 = d\phi/ds, \quad k_2 = (\sin \phi)/r \tag{7}$$

respectively.

The ratio of corresponding volume elements $(g/G)^{1/2}$ arising from the deformation is given by

$$(g/G)^{1/2} = (1 + (k_1 + k_2)n + k_1 k_2 n^2) v_3 (a/A)^{1/2} \tag{8}$$

where $(a/A)^{1/2}$ is the ratio of corresponding middle surface element areas and is given by

$$(a/A)^{1/2} = \lambda_1 \lambda_2. \tag{9}$$

For incompressible materials, we have

$$(g/G)^{1/2} = 1. \tag{10}$$

Substituting eqns (9), (10) and (5) into eqn (8) and integrating through the plate thickness yields

$$N = \lambda_1 \lambda_2 \left(n + \frac{(k_1 + k_2)}{2} n^2 + \frac{k_1 k_2}{3} n^3 \right) \tag{11}$$

which by reversion of series formulae can be rewritten to yield

$$n(N) = N/\lambda_1\lambda_2 - [(k_1 + k_2)/2] (N/\lambda_1\lambda_2)^2 + [(k_1 + k_2)^2/2 - k_1 k_2/3] (N/\lambda_1\lambda_2)^3 + \cdots \tag{12}$$

The deformation is completely specified by eqns (6), (7) and (12).

We assume the material to be *hyperelastic*; that is, we assume that it has a strain energy density function ω which depends only on the current, local, strain state. The mechanical properties of the material can thus be incorporated through ω. The Mooney–Rivlin strain energy function

$$\omega = C_1(I_1 - 3) + C_2(I_2 - 3) \tag{13}$$

where C_1, C_2 are material constants

$$I_1 = v_1^2 + v_2^2 + v_3^2, \quad I_2 = v_1^2 v_2^2 + v_2^2 v_3^2 + v_3^2 v_1^2 \tag{14}$$

and

$$v_3 = 1/v_1 v_2 \tag{15}$$

is assumed here. The constants C_1, C_2 can, if desired, be chosen to model small-strain linear response (with $\nu = 0.5$)—a feature which will allow subsequent comparison of results obtained here with the results for linear materials contained in the literature.

It is advantageous to cast the problem in terms of total potential energy P. The strain energy component W of P is given by

$$W = \int_S \mathscr{W}\, d(A^{1/2}) = \int_V \omega\, d(G^{1/2}) \tag{16}$$

where V denotes the undeformed plate volume and

$$\mathscr{W} = \int_{h/2}^{h/2} \omega(N)\, dN. \tag{17}$$

Equation (17) follows from standard arguments including use of eqn (15) to eliminate v_3. Substitution of eqns (5) and (12)-(14) into eqn (17) followed by simplifications common to thin-plate theory yields

$$\begin{aligned}\mathscr{W} = {} & C_1\{[\lambda_1^2 + \lambda_2^2 + \lambda_1^{-2}\lambda_2^{-2} - 3]h + [k_1^2(\lambda_2^{-2} + 3\lambda_1^{-4}\lambda_2^{-4}) \\ & + 4k_1k_2\lambda_1^{-4}\lambda_2^{-4} + k_2^2(\lambda_1^{-2} + 3\lambda_1^{-4}\lambda_2^{-4})]h^3/12\} \\ & + C_2\{[(\lambda_1^2 - k_1^2\lambda_2^{-2}h^2/4)^{-1} + (\lambda_2^2 - k_2^2\lambda_1^{-2}h^2/4)^{-1} \\ & + \lambda_1^2\lambda_2^2 - 3]h + [k_1^2 + 4k_1k_2 + k_2^2]h^3/12\}.\end{aligned} \tag{18}$$

This is a constitutive equation

$$\mathscr{W} = \mathscr{W}(\lambda_\alpha, k_\alpha) \tag{19}$$

for the middle surface of the plate. It is valid for arbitrarily large strains provided that radii of curvatures in the deformed state are large compared to the deformed plate thickness. A similar approach has been used by Simmonds[9], Taber[10], and Brodland and Cohen[11, 12] to derive large-strain constitutive equations for axisymmetric shells. For $C_2 = 0$, eqn (18) reduces to Simmond's eqn (28), suggesting that the thin-plate simplifications used here may be equivalent to the somewhat different simplifying assumptions used there.

Stresses based on the initial area are given by

$$\sigma_i^* = \frac{\partial \omega}{\partial \lambda_i}. \tag{20}$$

The ratio of the deformed differential area to the undeformed differential area is given by $1/\lambda_i$. Thus, a correction based on the area over which σ_i^* acts must be made when strains are large. The true stress is given by

$$\sigma_i = \lambda_i \sigma_i^* = \lambda_i \frac{\partial \omega}{\partial \lambda_i}. \tag{21}$$

True stress σ_i is used herein unless noted otherwise. Membrane stresses σ_1^m and σ_2^m in the meridian and hoop directions, respectively, are calculated at N = 0. Bending stresses σ_1^b and σ_2^b in the meridian and hoop directions are taken as the difference between the stress at N = h/2 and the corresponding membrane stress.

The *total potential energy P* of the deformed plate is given by

$$P = W - Q \tag{22}$$

where Q is the potential of the uniform transverse load q and is given by

$$Q = 2\pi q \int_0^a r\, w(r)\, dr \tag{23}$$

in terms of axial displacement w(r).

The deformed equilibrium configuration is determined using the variational principle that *deformed equilibrium configurations correspond to local stationary values of the total potential energy*. It is not, in general, possible to use even the simplified integral (16a) in conjunction with eqn (22) and the variational principle to analytically determine the deformed plate meridian. Appropriate numerical techniques, however, solve this problem easily.

3. NUMERICAL ANALYSIS

Let the meridian be broken into a series of discrete pieces as shown in Fig. 2. The n segmental functions S_j are pieced together between the n+1 nodes to satisfy the radial, axial and angular positions r_j, z_j and ϕ_j of the nodes. Specification of segmental functions S_j by

$$\eta_j(\xi) = \{\alpha_{j1}\xi(1-2\xi+\xi^2)+\alpha_{j2}\xi(-\xi+\xi^2)\}l_j \tag{24}$$

in terms of local Cartesian coordinates η, ξ using

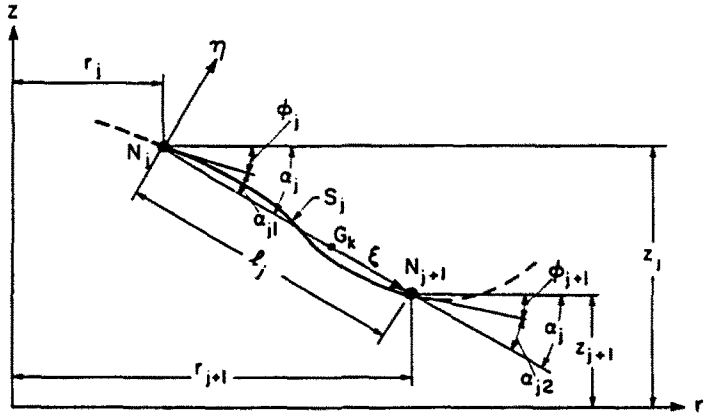

Fig. 2. Segmental representation.

$$\alpha_j = \tan^{-1}\{-(z_{j+1}-z_j)/(r_{j+1}-r_j)\} \tag{25}$$

$$l_j = \{(r_{j+1}-r_j)^2+(z_{j+1}-z_j)^2\}^{1/2} \tag{26}$$

and

$$\alpha_{j1} = \alpha_j - \phi_j, \quad \alpha_{j2} = \alpha_j - \phi_{j+1} \tag{27}$$

provides a piecewise cubic representation of the meridian, and allows the problem to be cast in terms of the $3(n+1)$ nodal positions r_j, z_j and ϕ_j ($j = 1$ to $n+1$) or X_i ($i = 1$ to $3(n+1)$). Since the transverse displacement $\eta_j(\xi)$ with respect to the *local* $\eta-\xi$ coordinate system can be assumed small compared with l_j, the meridian angle ϕ and curvature k_1 are given by

$$\phi(\xi) = \alpha_j - \frac{1}{l_j}\frac{d\eta_j(\xi)}{d\xi} \tag{28}$$

and

$$k_1(\xi) = -\frac{1}{l_j^2}\frac{d^2\eta(\xi)}{d\xi^2}. \tag{29}$$

Radial and axial positions, principal stretches and parallel curvature are given by

$$r(\xi) = (1-\xi)r_j + \xi r_{j+1} + \eta(\xi)\sin\alpha_j \tag{30}$$

$$z(\xi) = (1-\xi)z_j + \xi z_{j+1} + \eta(\xi)\cos\alpha_j \tag{31}$$

$$\lambda_1 = l_j/L_j, \quad \lambda_2 = r(\xi)/R(\xi) \tag{32}$$

and

$$k_2 = \sin\phi(\xi)/r(\xi). \tag{33}$$

The total strain energy integral is one-dimensional under axisymmetric deformations and can be written as

$$W = 2\pi\int_0^a r\mathscr{W}\,dr. \tag{34}$$

This integral can be evaluated in terms of nodal positions X_i using eqns (24)–(33) and Gaussian quadrature, which for p Gauss points, G_k, per segment, takes the form

$$\mathscr{W} = 2\pi\sum_{j=1}^{n}\sum_{k=1}^{p} r(G_k)f_k\mathscr{W}(G_k) \tag{35}$$

where f_k are Gaussian weighting factors. Substitution of eqn (35) into eqn (22) yields a total strain energy of the form

$$W = W(X_i) = W(\mathbf{X}). \tag{36}$$

Similarly, the potential Q of the transverse load q can be evaluated in terms of nodal positions using eqns (23) and (31) to yield

$$Q = Q(\mathbf{X}). \tag{37}$$

The total potential energy can then be written as

$$P = P(\mathbf{X}_i) = P(\mathbf{X}). \tag{38}$$

The problem is thus reduced to the form of a *non-linear programming problem* in that the stationary values of an objective function P, which cannot be written as a bilinear form in $\mathbf{X}$, are to be found in terms of $\mathbf{X}$. A host of techniques exist for the solution of this problem. A sequential gradient technique of the form

$$\mathbf{d} = -\mathbf{H}^{-1}\mathbf{g} \tag{39}$$

where

$$\mathbf{g} = \text{grad } P, \quad \mathbf{H} = \text{grad}^2 P \tag{40}$$

and $\mathbf{d}$ is a calculated displacement vector to a better estimate $\mathbf{X}+\mathbf{d}$, is satisfactory. The process can be accelerated by using a displacement $\alpha\mathbf{d}$ where α is determined by trial and error to minimize P along $\mathbf{X}+\alpha\mathbf{d}$. This so-called *line search* procedure is numerically efficient, as multiple evaluation of $P(\mathbf{X}+\alpha\mathbf{d})$ requires considerably less computer time than calculation of $\mathbf{d}$.

4. RESULTS AND DISCUSSION

The linear solutions, the non-linear analytical solutions of Way[13] and Berger[14], the membrane solution of Hencky[15], and the numerical solutions developed herein are considered over their respective domains. Since the results of Brodland ($a/h \geqslant 400$) and Way would be graphically indistinguishable over their common domain in Figs 3, 4 and 6, a solid line is used to represent both. In such figures the results of Brodland cover the full domain of the graph. The domain of Way's original results is indicated on Figs 3 and 4. Results calculated by Brodland using Way's method up to approximately $Q = 300$ are also indicated.

4.1. *Thin plates*

Figure 3 shows the load–center deflection behavior of a very thin hinged plate. Note that log–log axes are used. The Way and Berger plate solutions and the Hencky membrane solution are subject to the limitations of the von Karman equations, i.e. small strains and rotations. The solution developed herein agrees with these solutions when the plate is thin ($a/h \geqslant 400$).

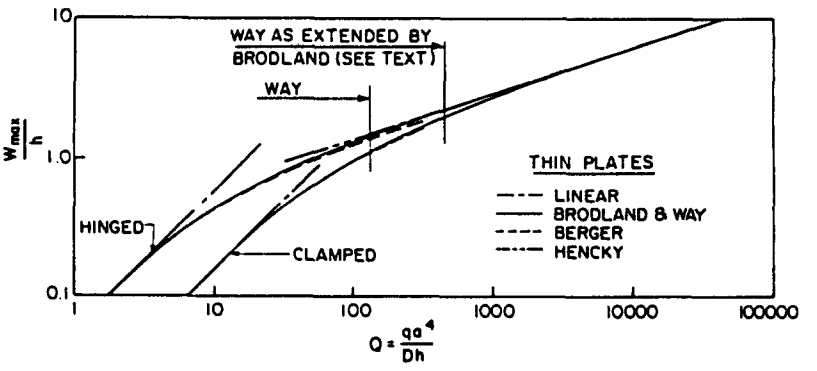

Fig. 3. Center deflection vs load.

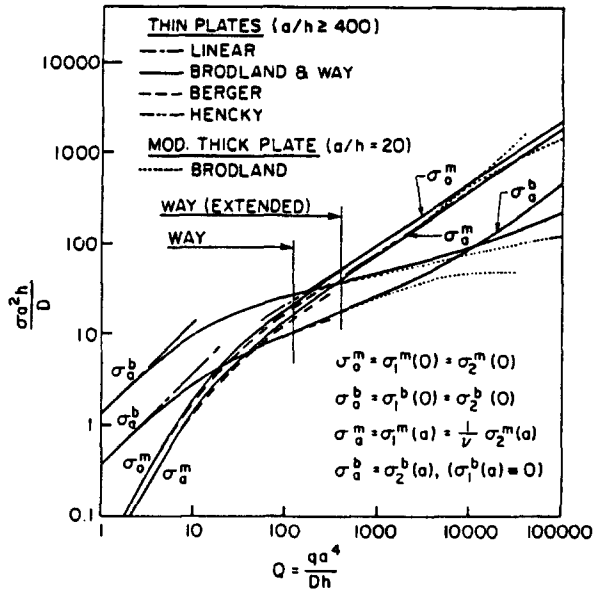

Fig. 4. Stress vs load for a hinged plate.

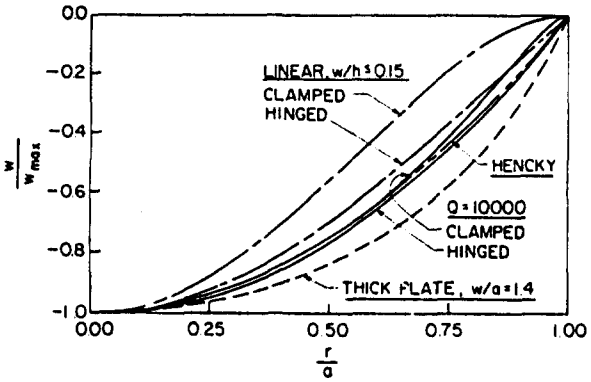

Fig. 5. Normalized deflection profiles.

A stress analysis reveals how the mechanism of load carrying changes with increasing load. Figure 4 shows that membrane stresses σ^m are nearly a magnitude less than bending stresses σ^b at $Q = 2$, and become even less significant with decreasing load. Thus, load is carried almost exclusively by plate *bending* in this range. The load range $2 < Q < 1000$ is transitional; membrane effects become increasingly important compared to bending stresses until at $Q \approx 12$, sufficient geometric changes have occurred that the load is carried equally by bending and membrane modes, and bending and membrane stresses are of the same magnitude. At a load of $Q = 1000$, bending stresses are about a third as large as membrane stresses. Their influence on the plate seems, however, to be slight, and the membrane mode of support predominates.

Figure 5 shows normalized deflection contours calculated using the linear solution, Hencky's solution, and determined numerically for $Q = 10{,}000$. Note that the *normalized* deflection contours (i.e. the plate *shapes*) predicted by the linear solution and by Hencky's solution do not depend on the value of Q. It is clear that the shape of a thin hinged plate changes surprisingly little with load.

The center deflection of a thin *clamped* plate is also shown in Fig. 3. Its center and edge stresses are shown in Fig. 6. For small loads $Q < 10$ and correspondingly small deflections, it is clear that the load is carried primarily by bending. Because the clamped plate is more severely restrained than a similar hinged plate, it deflects less for a given load. The linear behavior of both plates is limited by deflections of $w/h \simeq 0.15$. A transition from load carrying by bending to load carrying primarily by membrane effects occurs over

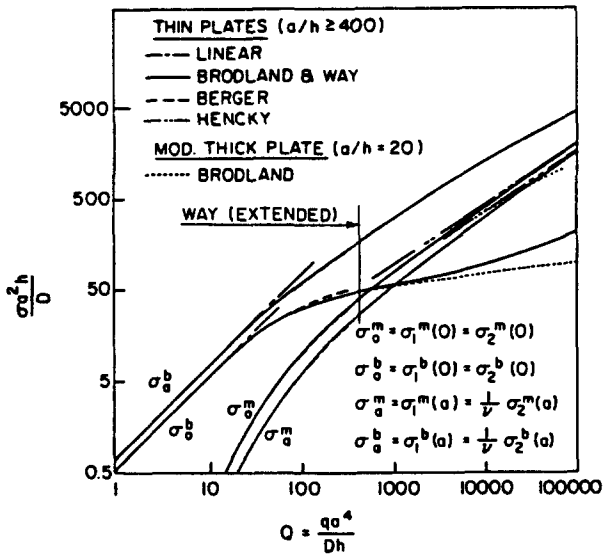

Fig. 6. Stress vs load for a clamped plate.

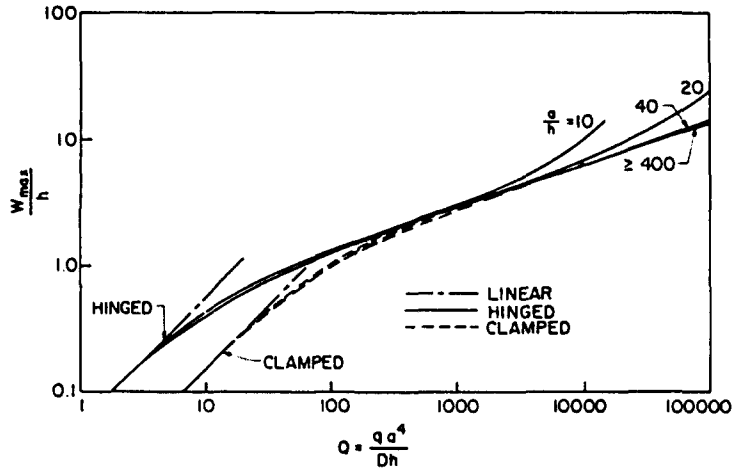

Fig. 7. Deflection of moderately thick plates.

$10 < Q < 5000$. For loads higher than $Q = 5000$, the deflections and membrane stresses in a clamped plate approach those in a hinged plate or a membrane.

Figure 5 shows that the normalized profile of a clamped plate changes much more with applied load than that of a hinged plate. For very large loads, the profiles of clamped and hinged plates become quite similar, and both approach the shape of a uniformly-loaded membrane.

Stress and deflection profiles for hinged and clamped plates with $Q = 120$ and 300 are given in Brodland[5]. These profiles also describe moderately thick plates; e.g. $a/h = 20$. Strains and rotations are still small in moderately thick plates at these loads and their behavior is therefore like that of thin plates.

4.2. *Moderately thick plates*

When loads are high and a plate is not very thin, rotations and strains are no longer small. For example, the maximum center deflections shown in Fig. 7 for plates with $a/h = 10$ and 20 are 1.4 times the plate radius. Membrane strains are approximately 80% and edge rotations are nearly 90°. (In contrast, the maximum strains and rotations in a thin plate ($a/h \geqslant 400$) for $Q = 100{,}000$ are only 0.1% and 4°, respectively.)

The von Karman equations do not adequately describe deflections as large as these because the assumptions used in their derivation are no longer valid. For example, when $du/dr = 0.3$ and $dw/dr = 1.4$, the meridional strain estimate

$$\varepsilon_r = \sqrt{\left(\left(1+\frac{du}{dr}\right)^2+\left(\frac{dw}{dr}\right)^2\right)}-1 \approx \frac{du}{dr}+\frac{1}{2}\left(\frac{dw}{dr}\right)^2 \tag{41}$$

used in the von Karman equations yields a value which is nearly 40% too large. In addition, when meridian rotations are this large, the assumed equivalence of quantities given in Lagrangian and Eulerian coordinates is in error by as much as 50%. It is, incidentally, these two simplifications which make the von Karman equations independent of the geometric parameter a/h (see Brodland[5] or Fung[16]). Discernable discrepancies begin to appear between the von Karman solutions and the numerical solutions in clamped plates as early as Q = 1000, and in hinged plates when Q is as low as 500 when a/h = 20 (see Figs 4, 6 and 7).

The Reissner equations are valid when rotations are large but strains are still small. They would thus adequately describe the behavior of a hinged or clamped plate with a/h = 20 up to approximately Q = 10,000, at which point strains and rotations have reached 10% and 30°, respectively. The Reissner equations would extend the range of valid solutions beyond the range of those based on the von Karman equations even more, when radial constraints are not so strong (e.g. an annulus with an edge load[1]) and large rotations can occur long before strains become large.

When strains and rotations are both large, deflections and stresses are significantly different from those predicted by the von Karman equations. For example, Fig. 7 shows the effect of a/h on the center deflection of both clamped and hinged plates. Numerical results for $a/h \geqslant 400$ compare very well with the various analytical solutions to the von Karman equations. For high loads, Q, and smaller values of a/h, the ratio of center deflection, w_{max}, to plate radius becomes significant, even for moderate values of w_{max}. For example, if a/h = 40 and Q = 100,000, then $w_{max}/h = 14.2$, and the ratio w_{max}/a is approximately 0.35. The deflection is 10% more than that predicted by the von Karman equations for a thin plate. The discrepancies between the thin and moderately thick plate solutions are more pronounced for a/h = 20; and for a/h = 10 the numerical solutions diverge from the thin plate solutions shortly after the range of linear theory ($w_{max}/h \leqslant 0.15$) is past. When $w_{max}/h > 3$ a uniformly loaded plate behaves like a membrane with respect to deflections and stresses, except within the boundary layer which develops when the edge is clamped. For a discussion of this boundary layer, see Refs [2, 5, 17].

Axial load is carried by meridional stress N_1 and shear stress Q_1 according to

$$N_1 \sin\theta - Q_1 \cos\theta = \frac{qr}{2}. \tag{42}$$

When rotations are small, a significant part of the axial load is carried by shear stress Q_1. When rotations are large, as they are in moderately thick plates under high load, the load-carrying capacity of Q_1 is much reduced because of the $\cos\theta$ term in eqn (42), and as a result, the meridional membrane stress N_1 must carry the bulk of the axial load. Figure 8 shows that the meridional membrane stress σ_1^m in a moderately thick hinged plate (a/h = 20) increases significantly toward its outer edge as a result of this rotational effect. Membrane stresses in a clamped plate with the same load and geometric proportions are virtually identical except within the boundary layer at the clamped edge. Figure 8 also shows that the strain condition $\varepsilon_2(a) = 0$ associated with a radially restrained edge does not imply that

$$\sigma_1^m(a) = \frac{1}{\nu}\sigma_2^m(a) \tag{43}$$

in a Mooney–Rivlin material *when strains are large*.

Membrane stresses are further increased by the thinning of the plate. Figure 8 shows membrane stretches λ_1 and λ_2. Their product $(\lambda_1\lambda_2)$ is inversely proportional to the plate thickness. The plate thus sustains a nearly uniform thickness reduction to approximately 1/1.30 of its original thickness. Figure 8 shows a stress measure σ_1^* based on the normal

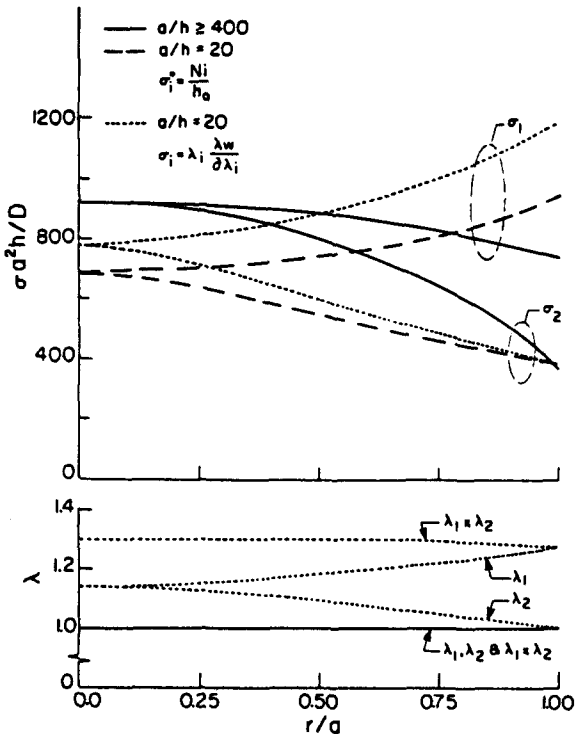

Fig. 8. Membrane stress and stretch profiles for Q = 30,000.

load resultant N_i and the *initial* thickness $h(h_0)$ (see eqn (20)). This stress can be thought of as a normalized, meridional membrane *load*. Membrane strains are sufficiently small in a *thin* plate ($\lambda_1 \approx \lambda_2 \approx \lambda_1 \times \lambda_2 \approx 1$ as shown in Fig. 8(b)) that both stress definitions produce the same stress value. Clearly, the membrane *load* is also lower at the plate center and higher at its edge compared to a thin plate. In contrast, plate thinning generally reduces bending stresses, as shown in Figs 4 and 6. Similar middle surface shape and stress dependence in pressure-loaded plates has been reported by Taber[2]. Both the large-rotation and large-strain (thinning) effects cause the normalized deflection of a thick plate to be greater than in a thin plate (see Fig. 7). Shear-related deformations have been neglected in this analysis. Their contribution to the total deflection of a moderately thick plate, however, can be significant.

The calculated meridional radius of curvature ($1/k_1$) at the edge of a clamped plate with a/h = 20 and Q = 30,000 is nearly as large as the (deformed) plate thickness. Thus, the curvature assumptions used in the derivation of the plate theory are violated and calculated stresses and deflections in this region are not reliable (see also Taber[10]). Edge stresses for moderately thick clamped plates are therefore not shown in Fig. 6.

The large strains, rotations and curvatures demonstrated here underscore the need for practical, large-strain plate and shell theories. Violation of the curvature assumptions ($|1/k_i| > 10h$) used in the plate theory developed herein, at the edge of a clamped plate, suggest the need for large-strain plate theories which are even more general.

The maximum deflections shown in Fig. 7 for a/h = 10 and 20 correspond to center deflections of 1.4 times the plate radius and loads of $qah^2/D = 14$. Both hinged plates have the *same middle surface shape* (see Fig. 5). When deflections, and hence strains and rotations, are this large, better similarity between solutions is provided by load parameter qah^2/D and corresponding dimensionless transverse deflections w/a. Identical middle surface shapes are then produced at high loads qah^2/D, and the ratio between shear stress σ^s and membrane stress σ^m is maintained since their dimensionless forms $\sigma^s h^3/D$ and $\sigma^m h^3/D$ are the same. The more usual load parameter qa^4/Dh and dimensionless deflection w/h maintain the ratio between bending stresses $\sigma^b a^2 h/D$ and membrane stresses $\sigma^m a^2 h/D$—factors which govern the small-strain deflection of plates—instead. When strains and rotations are high the deformation is governed by membrane and shear resultants rather than by bending, and

the load parameter qah^2/D is more suitable. Loads $qa^4/Dh = qah^2D(a/h)^3$ would be extreme in very thin plates ($a/h \geq 400$) before this situation would occur; i.e. $qah^2/D \sim 10$. Thus, although a distinction should really be made between small-strain and large-strain plate behavior, within the load domain $qa^4/Dh \leq 100{,}000$ a distinction based on relative plate thickness a/h is essentially equivalent.

Since incompressible materials have been assumed here, the effect of ν has not been studied. Its effect on the solution is shown in Refs [5, 13]. Changes to the material constants C_1, C_2 to model materials which become more or less stiff with increasing strain produces corresponding moderate changes in the load–deflection curves.

Acknowledgements—The author gratefully acknowledges the guidance provided by Dr H. Cohen of the University of Manitoba, and the financial support provided by the Natural Sciences and Engineering Research Council of Canada.

REFERENCES

1. V. G. Hart and D. J. Evans, Non-linear bending of an annular plate by transverse edge forces. *J. Math. Phys.* **43**, 275–303 (1964).
2. L. A. Taber, Nonlinear asymptotic solution of the Reissner plate equations. *ASME J. Appl. Mech.* **52**, 907–912 (1985).
3. E. Reissner, On finite deflections of circular plates. *Proc. Symp. Appl. Math.* **1**, 213–219 (1947).
4. G. J. Turvey and G. T. Lim, Axisymmetric full-range analysis of transverse pressure-loaded circular plates. *Int. J. Mech. Sci.* **26**(9/10), 489–502 (1984).
5. G. W. Brodland, Nonlinear deformation of uniformly loaded circular plates. *Solid Mech. Arch.* **11**(4), 219–256 (1986).
6. D. Yu. Panov and V. I. Feodos'ev, On the equilibrium and stability loss of shallow shells under large deflection. *Prikl. Mat. Mekh.* No. 4, 389–406 (1948).
7. C. Y. Chia, *Nonlinear Analysis of Plates*. McGraw-Hill, New York (1980).
8. L. H. Donnell, *Beams, Plates and Shells*. McGraw-Hill, New York (1976).
9. J. G. Simmonds, The strain-energy density of rubber-like shells of revolution undergoing torsionless, axisymmetric deformation (axishells). *ASME J. Appl. Mech.* **53**, 593–596 (1986).
10. L. A. Taber, On approximate large strain relations for a shell of revolution. *Int. J. Non-linear Mech.* **20**, 27–39 (1985).
11. G. W. Brodland and H. Cohen, Large-strain axisymmetric deformation of cylindrical shells. *ASME J. Appl. Mech.* **54**, 287–291 (1987).
12. G. W. Brodland and H. Cohen, Deflection and snapping of spherical caps. *Int. J. Solids Structures* **23**, 1341–1356 (1987).
13. S. Way, Bending of circular plates with large deflection. *Trans. A.S.M.E.* **56**, 627–636 (1934).
14. H. M. Berger, A new approach to the analysis of large deflection of plates. *J. Appl. Mech.* **22**, 465–472 (1955).
15. H. Hencky, Uber den Spannungszustand in kreisrunden Platten mit verschwindender Biegungssteifigkeit. *Z. Math. Phys.* **63**, 311–317 (1915).
16. Y. C. Fung, *Foundations of Solid Mechanics*, Prentice-Hall, Englewood Cliffs, New Jersey (1965).
17. E. Bromberg, Nonlinear bending of a circular plate under normal pressure. *Commun. Pure Appl. Math.* **9**, 633–659 (1956).